Quantum Hall Mach-Zehnder interferometer far beyond equilibrium

E. V. Deviatov,[1,*] A. Ganczarczyk,[2] A. Lorke,[2] G. Biasiol,[3] and L. Sorba[4]
[1]*Institute of Solid State Physics RAS, Chernogolovka, Moscow District 142432, Russia*
[2]*Laboratorium für Festkörperphysik, Universität Duisburg-Essen, Lotharstrasse 1, D-47048 Duisburg, Germany*
[3]*IOM CNR, Laboratorio TASC, I-34149 Trieste, Italy*
[4]*NEST, Istituto Nanoscienze–CNR and Scuola Normale Superiore, I-56127 Pisa, Italy*
(Received 8 June 2011; revised manuscript received 5 October 2011; published 27 December 2011)

We experimentally realize a quantum Hall Mach-Zehnder interferometer that operates far beyond equilibrium. The operation of the interferometer is based on allowed intraedge elastic transitions within the same Landau sublevel in the regime of high imbalances between the copropagating edge states. Since every edge state is definitely connected with a certain Landau sublevel, the formation of the interference loop can be understood as a splitting and a further reconnection of a single edge state. We observe an Aharonov-Bohm type interference pattern even for small-size interferometers. This interference scheme demonstrates high visibility even at millivolt imbalances and survives in a wide temperature range.

DOI: 10.1103/PhysRevB.84.235313 PACS number(s): 73.40.Qv, 71.30.+h

I. INTRODUCTION

Recent investigations of quantum Hall (QH) interferometers[1–16] give rise to several fundamental puzzles even in the integer QH regime. The major ones are the influence of the electron-electron interaction on the interference pattern[10,15,17] and the nature of the decoherence.[2,7,16]

Quantum Hall interferometers are realized[1] by current-carrying edge states[18] (ESs), arising at the intersections of the Fermi level and filled Landau levels at the sample edge. Usually, a key part of the interferometer scheme is a quantum point contact (QPC), which enables a connection between two identical counter-propagating edge states.[19] By using two QPCs in a proper sequence, an electronic analog of a Mach-Zehnder[1–8] or Fabry-Perot[9–16] interferometer can be realized.

The interference pattern reflects the operation regime of a quantum interferometer.[17] In the simplest case of the extreme Aharonov-Bohm (AB) regime, electron-electron interaction has no effect on the interference pattern. The interference period corresponds to the change of the flux $\Phi = BS$ through the interferometer loop area S by one flux quantum Φ_0, where S is practically independent of the magnetic field B. In the opposite extreme Coulomb-dominated (CD) regime, Φ depends also on the number of particles within the loop because of Coulomb interaction.[17] The interference pattern reveals complicated structures in the (B,S) plane in between these two extreme regimes.[17] It was recently demonstrated[10,15] that the extreme CD and mixed AB-CD regimes are realized in small (about 2 μm size) devices,[10] while the extreme AB regime is realized for big (20 μm) QPC-based interferometers.[15]

Different mechanisms were proposed to explain coherence[20–25] in the QPC-based interferometers. The coherence length was found[7,8,16] to be inversely proportional to the temperature, which is compatible with theoretical predictions based on a dephasing arising from the thermal noise of the environment.[8] However, the complete theory is still incomplete for the dependence of the dephasing on magnetic field and imbalance.[16]

Visibility of the interference oscillations can be seriously suppressed even by low (on the order of microvolts) voltage imbalances in QPCs.[2–9,16] In contrast, a clear visible interference was reported even at millivolt imbalances for the interferometers realized by two copropagating ESs at a single sample edge.[26,27] The evident discrepancy of the results implies a substantially different operation principle for the interferometers realized by copropagating ESs.

Here, we experimentally realize a quantum Hall Mach-Zehnder interferometer that operates far beyond the equilibrium. The operation of the interferometer is based on allowed intraedge elastic transitions within the same Landau sublevel in the regime of high imbalances between the copropagating edge states. Since every edge state is definitely connected with a certain Landau sublevel, the formation of the interference loop can be understood as a splitting and a further reconnection of a single edge state. We observe an Aharonov-Bohm type interference pattern even for small-size interferometers. This interference scheme demonstrates high visibility even at millivolt imbalances and survives in a wide temperature range.

II. SAMPLES AND TECHNIQUE

Our samples are fabricated from a GaAs/AlGaAs heterostructure grown by molecular beam epitaxy. It contains a two-dimensional electron gas (2DEG) located 200 nm below the surface. The 2DEG mobility at 4 K is 5.5×10^6 cm^2/V s and the carrier density is 1.43×10^{11} cm^{-2}.

The sample design realizes a quantum Hall interferometer based on independently contacted copropagating edge states; see Fig. 1. Edge states arise at the sample edges as the intersections of the Fermi level and filled Landau sublevels.[18] At a bulk filling factor $\nu = 2$ there are two copropagating spin-split ESs along the ungated mesa edges. The main gate redirects the inner ES [see Fig. 1(a)] by depleting the 2DEG underneath to a lower filling factor $g = 1$. It allows independent contact of two copropagating ESs in the gate-gap region at the outer mesa edge. The gate finger at the center of the gate-gap region divides the inter-ES junction onto two junctions. We study samples with two different gate finger widths w =1 and 1.5 μm.

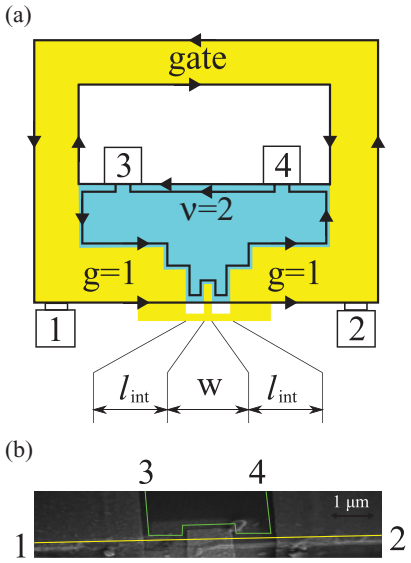

FIG. 1. (Color online) (a) Schematic diagram of the sample (not to scale). The outer sample dimension is about 2×2 mm^2. Each sample has a macroscopic ($\sim 0.5 \times 0.5$ mm^2) etched region inside. Ohmic contacts are placed at the mesa edges, denoted by bars with numbers. A split gate (light yellow) partially encircles the etched area, leaving uncovered a narrow gate-gap region at the outer mesa edge. The light green area indicates uncovered 2DEG. The w =1 or 1.5 μm width gate finger is placed at the center of the gate-gap, and is connected to the main gate outside the mesa. The lithographic overlap with the mesa is equal to $h = 0.3$ μm. The gate finger separates two ESs (thick lines) in the gate gap, so the inter-ES transitions are only allowed in two interaction regions of widths $l_{int} = 1$ μm. Arrows indicate electron propagation direction within the ES. (b) SEM image of the gate finger region. Two ESs (green and yellow thick lines) are sketched as straight lines, regardless of the roughness of the mesa edge. For measurements one of the inner contacts (3 or 4) is grounded. Current is applied to one of the outer contacts (1 or 2), while the other outer contact is used to trace the outer ES potential.

To study the transmittance of the device we ground one of the inner Ohmic contacts (3 or 4) and apply a dc current to one of the outer contacts (1 or 2). The other outer contact is used to trace the outer ES potential. We check that the obtained interference pattern does not depend on the particular choice of the contact combination, which only affects the total resistance of the device.

At positive currents, an electron contributes to transport only if it is transferred from the inner ES to the outer one in the gate-gap region. It can occur with some probability in the first ES junction of width $l_{int} = 1$ μm, or an electron can follow the inner ES around the gate finger and be transferred in the second one; see Fig. 1. In a very naive picture these two transmission regions serves as two semitransparent mirrors in an optical Mach-Zehnder interferometer, while two paths around the gate finger define the interferometer arms. This naive picture does not include sophisticated dependence of the inter-ES transport on ES imbalance at a single sample edge; see Ref. 28 for a review. We discuss the interferometer operation in detail after presenting the experimental results.

The phase difference $\phi = \Phi/\Phi_0$ between the interferometer arms is controlled by the flux Φ through the gate finger area. Φ can be affected[17] by varying either the magnetic field B or the effective gate finger area S. Within the QH plateau, S is sensitive to the *top* gate voltage V_g only because of variation of the depletion width along the gate perimeter. In contrast with commonly used plunger gates, S increases with further depletion of the top gate.

The measurements are performed in a dilution refrigerator with a minimal temperature of 30 mK. The interference pattern is independent of the cooling cycle. Standard two-point magnetoresistance is used to determine the regions of B that correspond to integer QH filling factors ν in the ungated area. We measure capacitance between the gate and the 2DEG as a function of the gate voltage V_g at constant magnetic field to find V_g regions of integer filling factors g under the gate.

III. EXPERIMENTAL RESULTS

To observe the interference effects in the transmittance of the device, we apply fixed dc current I in the range of 0.5–20 nA across the gate-gap junction as described before. The potential of the outer contact $V(B, V_g)$, shown in Fig. 2, depends on the magnetic field B (a) and the gate voltage V_g (b). Both B and V_g are varied within the $g = 1$ QH state under the gate finger. A monotonous increase in $V(B)$ is subtracted from the curve in Fig. 2(a). The curves in Fig. 2(b) remain unchanged. The $V(V_g)$ signal drops down at the edges of the $g = 1$ QH plateau [see also Fig. 3(a)], because at finite σ_{xx} under the gate some part of the current flows outside the gate-gap region.

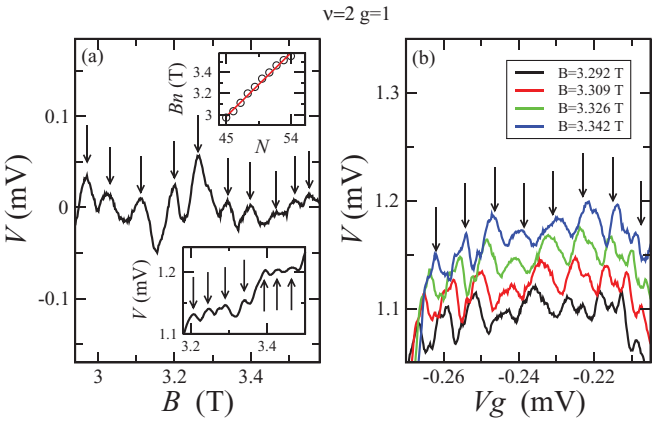

FIG. 2. (Color online) Examples of the oscillating behavior while sweeping the magnetic field B at constant gate voltage $V_g = -0.215$ V (a) or the gate voltage V_g at several constant magnetic fields (b) within the $g = 1$ QH state under the gate finger. Arrows indicate the positions of the oscillations. They are equidistant—see upper inset to part (a)—and their evolution demonstrates the extreme AB interference regime (b). The obtained periods are $\Delta B = 67$ mT and $\Delta V_g = 7.8$ mV, respectively. A monotonous increase in $V(B)$ is subtracted from the $V(B)$ curve in part (a). The curves in part (b) remain unchanged; the signal drops down at the $g = 1$ QH plateau edges [see also Fig. 3(a)]. Measurement current is $I = 4$ nA. The lower inset in part (a) demonstrates raw $V(B)$ oscillations with $\Delta B = 45$ mT for the $w = 1.5$ μm sample, $I = 10$ nA. Filling factors are $\nu = 2$ and $g = 1$.

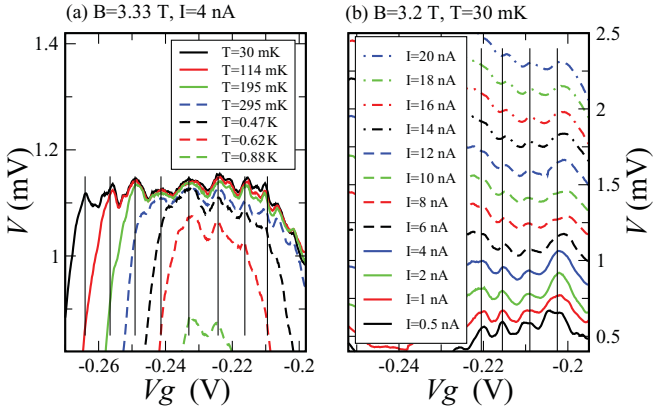

FIG. 3. (Color online) (a) Oscillations in V for different temperatures T. The oscillations amplitude is insensitive to the temperature, in contrast to the width of the $g = 1$ QH plateau and the mean level of the signal. The signal drops down at the $g = 1$ QH plateau edges. Measurement current is $I = 4$ nA, and magnetic field is $B = 3.33$ T. (b) Oscillations for different imbalances (measurement currents) at $B = 3.2$ T and $T = 30$ mK. The amplitude is practically independent of the imbalance. The mean value of the signal reflects the I-V dependence (the lowest curves are still shifted vertically in the figure to avoid overlap). Thick lines indicate the positions of the oscillations, which differ in (a) and (b) because of different fields.

Both the $V(B)$ and $V(V_g)$ dependencies exhibit nearly equidistant oscillations [see inset to Fig. 2(a)] with periods $\Delta B = 67$ mT and $\Delta V_g = 7.8$ mV, respectively. Figure 2(b) also shows the evolution of the oscillation picture with increasing magnetic field. The position of every oscillation moves to higher V_g with increasing magnetic field B. Since the increase in V_g lowers the depletion, it lowers S, so this behavior is a fingerprint of the extreme AB interference regime[17] $\phi = BS/\Phi_0$. This behavior is demonstrated for a wide magnetic field range.

Because of the simple relation $\phi = BS/\Phi_0$ in the extreme AB interferometer regime, ΔB reflects the whole active interferometer area S: $\Delta B = \Phi_0/S$. High values of the oscillation numbers $N = B/\Delta B$ in the inset to Fig. 2(a) also support the invariance of the loop area S while changing the flux Φ on a quantum Φ_0. The estimation $S = \Phi_0/\Delta B \approx 0.1\ \mu\text{m}^2$ is in a reasonable agreement with the gate finger dimensions, because the lithographic length $h = 0.3\ \mu$m should be corrected by a depletion length of roughly the 2DEG depth ($\approx$200 nm) at the mesa edge.[15,16,29] The sample with the bigger width $w = 1.5\ \mu$m demonstrates oscillations with $\Delta B = 45$ mT, which corresponds to $S = \Phi_0/\Delta B \approx 0.15\ \mu\text{m}^2$. Thus, the period ΔB reasonably scales with the gate finger width w even in view of the obvious roughness of the etched mesa edge.

The above-described picture of the extreme AB interference regime is also confirmed by measurements at other integer filling factors. Usually ΔB scales with filling factors for small QPC-based interferometers,[10] which is a characteristic feature of the CD interference regime.[17] In the present investigation, we obtain $\Delta B = 70$ mT for $\nu = 3$, $g = 1$, and slightly higher $\Delta B = 90$ mT for $\nu = 3$, $g = 2$ fillings. There are three ESs in the gate-gap junction at the bulk filling factor $\nu = 3$. Because at $g = 1$ there is one ES under the gate finger, the interferometer geometry is formed by the same two outer spin-split ESs as in the $\nu = 2$, $g = 1$ case. For $g = 2$, S is somewhat diminished because of two ESs under the gate finger, which is reflected in a higher period.

In contrast to previous investigations,[1–7,10–16] the interference is certainly demonstrated at millivolt imbalances in Fig. 2. Moreover, the interference oscillations appears only above some threshold imbalance value. Above this value, they are nearly independent of the applied imbalance; see Fig. 3(b). The oscillations also remain practically unchanged with increasing temperature in Fig. 3(a), while the $g = 1$ QH plateau width, as determined by the signal drop, is highly sensitive to the temperature. The oscillations are visible even at $T = 0.88$ K, where the plateau is very narrow and the level of the signal is diminished because of an admixture of the dissipative current under the gate finger; see Fig. 3(a).

IV. DISCUSSION

As a result, (i) we undoubtedly observe interference oscillations at millivolt imbalances in our device; (ii) the visibility of the oscillations does not depend on the imbalance and temperature; (iii) the interferometer operates in the extreme AB regime, i.e., electron-electron interaction has minor effect on the interference pattern. This behavior is strongly different from that reported for interferometers based on QPC.[1–7,10–16]

A. Evolution of I-V characteristics

To understand the origin of the interference oscillations at high imbalances, we consider I-V characteristics of the gate-gap junction.

Let us start from the I-V curve at constant B and V_g. A typical experimental I-V curve is shown in Fig. 4(a) for the filling factors $\nu = 2$, $g = 1$. At low imbalances, the positive I-V branch is characterized by high resistance, so the inter-ES transport is negligible. Above some threshold imbalance value V_{th} the resistance drops significantly, which indicates much higher transport. The negative I-V branch is strongly nonlinear and does not contain any specific points.[28]

Since the phase $\phi = \Phi/\Phi_0$ is practically independent of the imbalance at constant B and V_g [see Fig. 3(b)] we can expect I-V to be determined by the edge energy structure in the gate-gap junction, in complete similarity to the structures without the gate finger; see Refs. 28 and 30. The edge energy structure is depicted in Fig. 5(a) in the equilibrium.[29] In samples with a smooth edge profile, edge states[18] are represented by compressible strips of finite width,[29] located at the intersections of the Fermi level and filled Landau levels.

Applied inter-ES electrochemical potential imbalance modifies the potential jump between two ESs. It is slightly diminished for low positive imbalances, because of the polarity in our setup. The inter-ES transport is still negligible because the charge equilibration length[31] $l_{\text{eq}} \sim 100\ \mu$m exceeds significantly the total gate-gap junction width $2l_{\text{int}} = 2\ \mu$m. On the other hand, high positive inter-ES imbalance V seriously

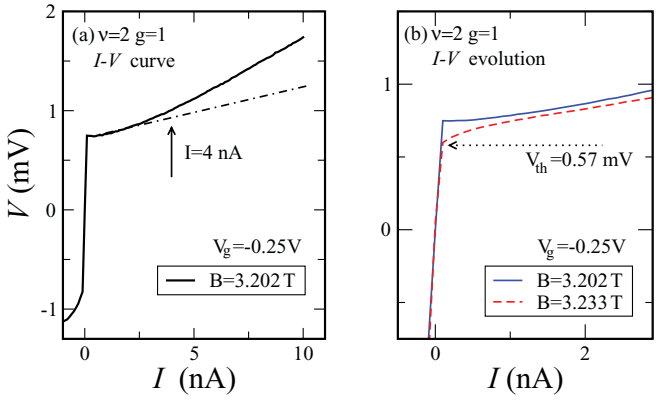

FIG. 4. (Color online) I-V curves of the gate-gap junction for transport between two spin-split ESs for the filling factors $\nu = 2$ and $g = 1$. (a) The I-V curve at constant $B = 3.203$ T and $V_g = -0.25$ V in a wide current range. The positive branch decreases its slope abruptly at $V_{\rm th}$ because of flattening of the potential jump between the two ESs; compare the energy diagrams in Figs. 5(a) and 5(b). The dash-dotted line indicate the equilibrium resistance $R_{\rm eq} = 2h/e^2$ above $V_{\rm th}$. The highly nonlinear negative branch is shown around the zero region only. (b) Evolution of the experimental I-V curve near $V_{\rm th}$ with small variation of the magnetic field B. The value $V_{\rm th} = 0.57$ mV obtained at $B = 3.233$ T coincides well with one for samples without a gate finger; see Ref. 30.

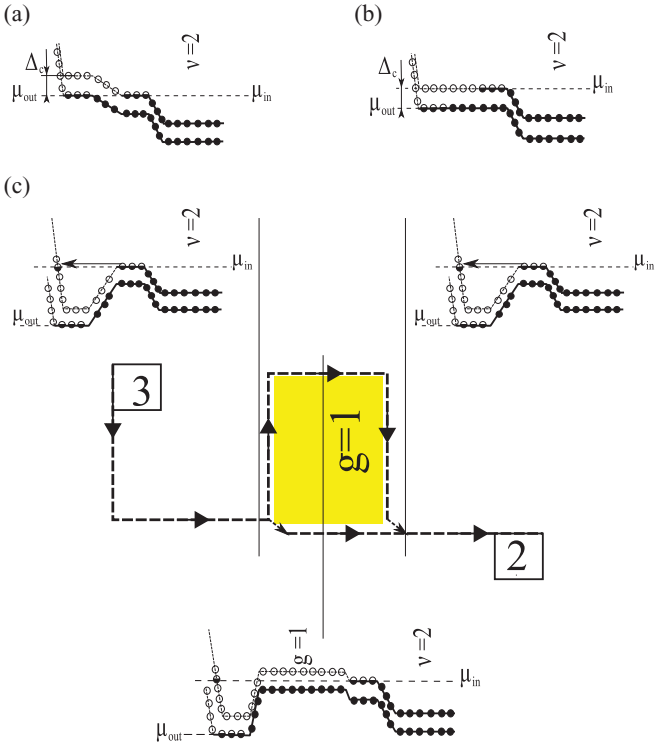

FIG. 5. (Color online) (a) Energy diagram in the gate-gap region in equilibrium[28] ($\mu_{\rm out} = \mu_{\rm in}$, no electrochemical potential imbalance is applied). Pinning[29] of the energy levels to the Fermi level (short-dashed line) is shown in the compressible regions (ESs). Half-filled circles indicate partially occupied electron states in the compressible strips. Filled (open) circles represent the fully occupied (empty) electron states. Δ_c is the potential jump between two ESs. (b) Flattening of the potential jump by the positive voltage V, with $eV = eV_{\rm th} = \mu_{\rm out} - \mu_{\rm in} = -\Delta_c$, $e < 0$. (c) An electron propagation around the interference loop in the gate finger area (light yellow). Energy diagrams are shown before the gate finger (left), across it (bottom), and after the gate finger (right) at high imbalances $V > V_{\rm th}$. Arrows indicate the intraedge elastic transitions without spin-flip.

distorts the edge energy structure.[28,30] It flattens the potential jump between two ESs at some value $V = V_{\rm th}$ [see Fig. 5(b)] which is reflected by the resistance drop in the experimental I-V curve. At higher imbalances the potential between ES is even more distorted, so the resistance still exceeds it equilibrium value;[28,30] see Fig. 4(a).

We want to emphasize that, despite the fact that the theory[29] was developed only for the equilibrium, the diagrams in Fig. 5 are qualitatively proven by the I-V curve spectroscopy.[28,30] For the samples without the gate finger, $V_{\rm th}$ simply reflects the Zeeman splitting at the edge, which is monotonically increasing with the magnetic field.[30] This is the reason for the monotonous increase in $V(B)$ that is subtracted from the curve in Fig. 2(a). The value $V_{\rm th} = 0.57$ mV obtained from the I-V curve at $B = 3.233$ T coincides well with one for the samples without the gate finger; see Ref. 30.

An example of the I-V evolution is shown in Fig. 4(b). We change the phase $\phi = \Phi/\Phi_0$ by low variation of the magnetic field B at a constant gate voltage. Two values of the magnetic field in Fig. 4(b) are close to the two neighboring maxima and minima in Fig. 2(a). The effect appears as a vertical shift of the curve at $V > V_{\rm th}$. For these two curves the shift is *negative* for the positive increase of the magnetic field, which is just opposite to the monotonous Zeeman increase of $V_{\rm th}$.

Figure 4(b) is another representation of the interference independence of the applied imbalance in Fig. 3(b). It clearly demonstrates that no interference effects can be seen below $V_{\rm th}$ in our experimental setup.

B. Interferometer operation

We now discuss the formation of the interference loop for an electron in detail. Figure 5(c) shows the energy diagrams for different positions within the gate-gap junction in Fig. 1.

If we consider the inter-ES transport to both sides of the gate finger, two major possibilities are allowed for an electron: (i) it can be directly transferred between the ground states in two ESs, which is accompanied by energy loss and a spin flip, i.e., by the coherence loss; (ii) at $V > V_{\rm th}$ an electron can be elastically transferred within the same energy sublevel [see Fig. 5(c)] with relaxation to the ground state afterward in the outer ES. The latter possibility preserves the coherence for the time scale smaller than the relaxation time.

Thus, if the gate finger width w is smaller than the relaxation length, an electron can cross the gate finger region by two paths, shown in Fig. 5(c): it encircles the finger gate along the inner ES or propagates along the outer mesa edge in the excited state (bottom diagram). These two paths form two arms of the interferometer loop, and are reconnected at the opposite finger edge.

We find it worth mentioning that an electron placed at any interferometer arm still belongs to the same Landau sublevel. Since every ES is definitely connected with a certain Landau sublevel, the formation of the interference loop can

be understood as a splitting and a further reconnection of the inner ES.

The proposed interferometer operation scheme is supported by experimental facts. We observe the interference oscillations only in the regime of allowed elastic transitions $V > V_{th}$; see, e.g., Fig. 4(b). In this regime, an electron is at the same energy for both interferometer arms. This energy is independent of the exact value of the inter-ES imbalance, which only slightly affects the position of the outer arm. The drift velocity for every arm is determined by the energy level slope, which is also insensitive to the bias applied *between* two compressible strips; see Fig. 5(c). Thus, the inter-ES imbalance can only have a minor effect on the oscillations, as we observe in the experiment; see Fig. 3(b). The proposed scheme is also independent of the temperature, as long as the temperature is much below eV_{th}, as demonstrated in Fig. 3(a).

C. Coherence

In the proposed interferometer scheme, based on elastic intraedge transitions, the coherence is first restricted by the relaxation of the nonequilibrium electron in Fig. 5(c).

The energy relaxation length was studied in Ref. 32 for low (microvolt) imbalances. It was found to exceed 10 μm, which is well above the gate finger widths $w = 1$ and 1.5 μm in our devices. On the other hand, the relaxation mechanism at high imbalances may be different. We can only estimate it to exceed 5 μm as an indirect result of the I-V curve spectroscopy investigations for samples with different gate-gap widths.[28]

For the QPC-based interferometers, the coherence length investigations[7,8,16] establish a dephasing that arises from the thermal charge noise of the environment.[8] However, the complete theory is still incomplete, even for low imbalances.[16] From the present experiment we cannot specify the decoherence mechanism, except for two statements: (i) the coherence is insensitive to the temperature as long as the temperature is much below eV_{th} [Fig. 3(a)]; and (ii) the decoherence mechanism connected with neutral collective modes[25] might be important because of allowed emission of these modes at high imbalances; see Ref. 33.

V. CONCLUSION

As a conclusion, we experimentally realize a quantum Hall Mach-Zehnder interferometer that operates far beyond the equilibrium. The operation of the interferometer is based on allowed intraedge elastic transitions within the same Landau sublevel in the regime of high imbalances between the copropagating edge states. Since every edge state is definitely connected with a certain Landau sublevel, the formation of the interference loop can be understood as a splitting and a further reconnection of a single edge state. We observe an Aharonov-Bohm type interference pattern even for small-size interferometers. This interference scheme demonstrates high visibility even at millivolt imbalances and survives in a wide temperature range.

ACKNOWLEDGMENTS

We wish to thank V. T. Dolgopolov and D. E. Feldman for fruitful discussions. We gratefully acknowledge financial support by the RFBR, the RAS, and the Program "The State Support of Leading Scientific Schools."

*dev@issp.ac.ru

[1] Y. Ji, Y. Chung, D. Sprinzak, M. Heiblum, D. Mahalu, and H. Shtrikman, Nature (London) **422**, 415 (2003).
[2] I. Neder, M. Heiblum, Y. Levinson, D. Mahalu, and V. Umansky, Phys. Rev. Lett. **96**, 016804 (2006).
[3] I. Neder, M. Heiblum, D. Mahalu, and V. Umansky, Phys. Rev. Lett. **98**, 036803 (2007).
[4] L. V. Litvin, H.-P. Tranitz, W. Wegscheider, and C. Strunk, Phys. Rev. B **75**, 033315 (2007).
[5] L. V. Litvin, A. Helzel, H.-P. Tranitz, W. Wegscheider, and C. Strunk, Phys. Rev. B **78**, 075303 (2008).
[6] Preden Roulleau, F. Portier, D. C. Glattli, P. Roche, A. Cavanna, G. Faini, U. Gennser, and D. Mailly, Phys. Rev. B **76**, 161309(R) (2007).
[7] P. Roulleau, F. Portier, D. C. Glattli, P. Roche, A. Cavanna, G. Faini, U. Gennser, and D. Mailly, Phys. Rev. Lett. **100**, 126802 (2008).
[8] P. Roulleau, F. Portier, P. Roche, A. Cavanna, G. Faini, U. Gennser, and D. Mailly, Phys. Rev. Lett. **101**, 186803 (2008).
[9] W. G. van der Wiel, Y. V. Nazarov, S. DeFranceschi, T. Fujisawa, J. M. Elzerman, E. W. G. M. Huizeling, S. Tarucha, and L. P. Kouwenhoven, Phys. Rev. B **67**, 033307 (2003).
[10] N. Ofek, A. Bid, M. Heiblum, A. Stern, V. Umansky, and D. Mahalu, Proc. Natl. Acad. Sci. **107**, 5276 (2010).
[11] F. E. Camino, Wei Zhou, and V. J. Goldman, Phys. Rev. Lett. **95**, 246802 (2005).
[12] F. E. Camino, Wei Zhou, and V. J. Goldman, Phys. Rev. B **76**, 155305 (2007).
[13] F. E. Camino, Wei Zhou, and V. J. Goldman, Phys. Rev. Lett. **98**, 076805 (2007).
[14] Ping V. Lin, F. E. Camino, and V. J. Goldman, Phys. Rev. B **80**, 125310 (2009).
[15] Y. Zhang, D. T. McClure, E. M. Levenson-Falk, C. M. Marcus, L. N. Pfeiffer, and K. W. West, Phys. Rev. B **79**, 241304 (2009).
[16] D. T. McClure, Y. Zhang, B. Rosenow, E. M. Levenson-Falk, C. M. Marcus, L. N. Pfeiffer, and K. W. West, Phys. Rev. Lett. **103**, 206806 (2009).
[17] B. I. Halperin, A. Stern, I. Neder, and B. Rosenow, Phys. Rev. B **83**, 155440 (2011).
[18] M. Büttiker, Phys. Rev. B **38**, 9375 (1988).
[19] For a review see A. Stern, Annals of Physics **323**, 204 (2008).
[20] K. T. Law, D. E. Feldman, and Yuval Gefen, Phys. Rev. B **74**, 045319 (2006).
[21] E. V. Sukhorukov and V. V. Cheianov, Phys. Rev. Lett. **99**, 156801 (2007).
[22] J. T. Chalker, Y. Gefen, and M. Y. Veillette, Phys. Rev. B **76**, 085320 (2007).

[23]I. Neder and E. Ginossar, Phys. Rev. Lett. **100**, 196806 (2008).
[24]S.-C. Youn, H.-W. Lee, and H.-S. Sim, Phys. Rev. Lett. **100**, 196807 (2008).
[25]Ivan P. Levkivskyi and Eugene V. Sukhorukov, Phys. Rev. B **78**, 045322 (2008).
[26]E. V. Deviatov and A. Lorke, Phys. Rev. B **77**, 161302(R) (2008).
[27]E. V. Deviatov, B. Marquardt, A. Lorke, G. Biasiol, and L. Sorba, Phys. Rev. B **79**, 125312 (2009).
[28]For a review on inter-ES transport see E. V. Deviatov, and A. Lorke, Phys. Status Solidi B **245**, 366 (2008).
[29]D. B. Chklovskii, B. I. Shklovskii, and L. I. Glazman, Phys. Rev. B **46**, 4026 (1992).
[30]E. V. Deviatov, A. Lorke, G. Biasiol, L. Sorba, and W. Wegscheider, JETP Lett. **92**, 69 (2010).
[31]G. Müller, D. Weiss, A. V. Khaetskii, K. von Klitzing, S. Koch, H. Nickel, W. Schlapp, and R. Lösch, Phys. Rev. B **45**, 3932 (1992).
[32]H. le Sueur, C. Altimiras, U. Gennser, A. Cavanna, D. Mailly, and F. Pierre, Phys. Rev. Lett. **105**, 056803 (2010).
[33]E. V. Deviatov, A. Lorke, G. Biasiol, and L. Sorba, Phys. Rev. Lett. **106**, 256802 (2011).